Exploring Rovibrational States of Floppy Molecules Using Diffusion Monte Carlo

Jason E. Ford

Honors Research Thesis

Presented in partial fulfillment of

the requirements for graduation

"with Honors Research Distinction in Chemistry"

from the

College of Arts and Sciences

at

The Ohio State University

Advisor: Professor Anne B. McCoy

April 17th, 2015

Abstract

In this work, diffusion Monte Carlo (DMC) methodology was extended to allow for the calculation of rotationally excited states by expansion into a functional space. This new methodology was used to study CH_5^+ and its deuterated isotopologues. Previous results regarding the localization of deuterium atoms within the H_3 subunit are corroborated, and new results regarding the lack of change in the wavefunction upon rotational excitation up to $J = 10$ are shown. The method was then tested concurrently with the previously established fixed node DMC method on H_2D^+ and HD_2^+, to determine its efficacy in capturing rovibrational coupling. This mixed method was found to produce errors up to 20 cm^{-1} for states with $J = 2$ and $\nu_{\text{asym}} = 1$. Group theory was then used to analyze the cause of the error, and showed the exclusion of Coriolis coupling terms to likely be at fault.

1 Introduction

The chemistry that takes place in the interstellar medium is very different from that which takes place on Earth. Floppy molecules, those that exhibit large amplitude motions even in their ground state, frequently form in this environment. This class of molecules contains exotic species such as H_2D^+ and CH_5^+ (pictured in Figure 2). The vibrations and rotations of these molecules differ greatly from what a simple harmonic oscillator or rigid rotor model predict.[1] Radio astronomical measurements provide evidence for chemical concentrations and temperatures by comparison to experimentally collected spectra of astrochemical species.[2] As can be seen in Figure 1, the rotationally resolved spectra of floppy molecules are often quite complex, and can be better understood when theoretical studies are paired with experiment.[3] The infrared spectra of these species provide an excellent opportunity for deepening the theoretical understanding of rotations and vibrations in astrochemical species as well as reactive intermediates in the atmosphere.[4] This type of spectrum can give insights into molecular structure, as well as the degree of rotation-vibration coupling, both of which can impact chemical reactivity. Calculations of ground and excited state energies can be used to assign a spectrum of this type with specific transitions.

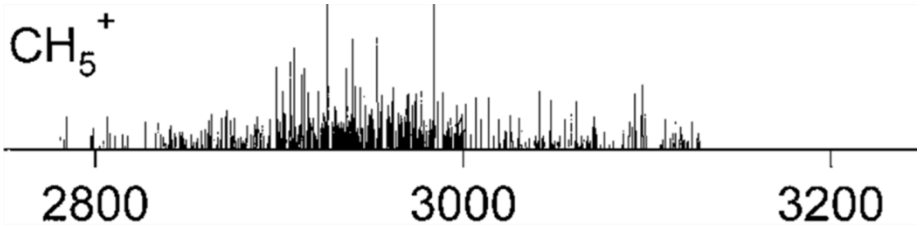

Figure 1: The infrared spectrum of CH_5^+, taken by Oka in 1999,[5] is exceptionally rich and difficult to understand with basic theories; energies are given in cm^{-1}

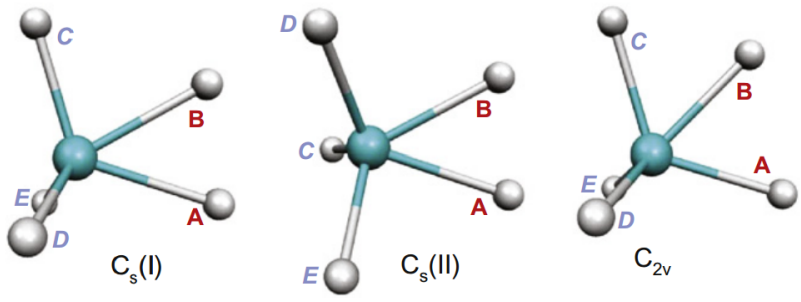

Figure 2: Three important geometries of CH_5^+; all of the hydrogen atoms may permute with one another, and each of these geometries are sampled in the ground state

Variational calculations are frequently an accurate method of determining transition energies, but the computational cost grows very quickly with system size, especially for floppy molecules. For small systems such as H_3^+ this is yet feasible, but for larger floppy systems such as CH_5^+, the calculations are very slow to converge.[6] Diffusion Monte Carlo (DMC), originally a ground state method, has been expanded to allow calculations of rotationally and vibrationally excited state energies and wavefunctions, providing a method for determining the transition energies encapsulated in a spectrum. This method has been used in many different capacities, from studies of electrons on 2-D surfaces, to quantum dots and bosonic gasses.[7–9] In recent history, there have been many applications of DMC to floppy molecules and systems, including HF dimers, Criegee intermediates, water clusters, and of course CH_5^+.[4,10–13]

2 Diffusion Monte Carlo

DMC takes advantage of the similarity between the Fick diffusion equation and the time-dependent Schrödinger equation and allows one to obtain the ground state energy and wavefunction of a quantum system. In one dimension:

$$\frac{\partial C}{\partial t} = D\frac{\partial^2 C}{\partial x^2} \tag{1}$$

$$-i\hbar\frac{\partial \Psi}{\partial t} = \frac{\hbar^2}{2m}\frac{\partial^2 \Psi}{\partial x^2} - V(x)\Psi \tag{2}$$

In these equations, C is a concentration gradient, t is time, D is the diffusion coefficient, x is position, i and $\hbar$ are fundamental constants, Ψ is the wavefunction, m is a particle's mass, and $V(x)$ is a potential function. Adding a linear term to the diffusion equation (kC) and converting the Schrödinger equation to imaginary time ($\tau = it/\hbar$) yields:

$$\frac{\partial C}{\partial t} = D\frac{\partial^2 C}{\partial x^2} - kC \tag{3}$$

$$\frac{\partial \Psi}{\partial \tau} = \frac{\hbar^2}{2m}\frac{\partial^2 \Psi}{\partial x^2} - V(x)\Psi \tag{4}$$

The isomorphism that has been constructed between the equations can be manipulated. The algorithm for DMC was laid out by Anderson in 1975.[14] In this approach, the wavefunction is expanded in an ensemble of weighted (W_i) 3N-dimensional Dirac delta-functions called walkers, N being the number of atoms in the system.

$$\langle \vec{R} | \Psi(\tau) \rangle = \sum_{i}^{N_{\text{walker}}} W_i(\tau) \delta^{3N} \left(\vec{R} - \vec{R}_i(\tau) \right) \tag{5}$$

The split operator approximation to the solution of the time-dependent Schrödinger equation is used to propagate the wavefunction in imaginary time:

$$|\Psi(\tau + \delta\tau)\rangle \approx e^{-(\hat{V} - E_{\text{ref}}(\tau))\delta\tau} e^{-\hat{T}\delta\tau} |\Psi(\tau)\rangle \tag{6}$$

In this ansatz, the kinetic energy operator leads to walker diffusion; each delta-function is displaced in each of its 3N dimensions by a random value. The random value is determined by a Gaussian distribution with a standard deviation, $\sigma = \sqrt{\delta\tau / m_k}$, where $\delta\tau$ is the time step and m_k is the mass of the kth atom in the system. The potential energy is obtained from an applicable potential energy surface. The additional reference energy term, E_{ref}, becomes the ground state energy while the distribution of walkers approaches the ground state wavefunction:

$$\Psi(\tau) = \sum_{n=0} c_n \psi_n \exp\left[-(E_n - E_{\text{ref}})\tau\right] \tag{7}$$

$$\Psi(\tau) = c_0\psi_0 + \sum_{n=1} c_n \psi_n \exp\left[-(E_n - E_{\text{ref}})\tau\right] \tag{8}$$

$$\lim_{\tau \to \infty} \Psi(\tau) = c_0 \psi_0 \tag{9}$$

The reference energy is calculated using the average potential energy of the walkers, $\bar{V}$, and a correction based on total weights, W_{total}, with an empirically determined coefficient, $\alpha = (2\delta\tau)^{-1}$:

$$E_{\text{ref}}(\tau) = \bar{V}(\tau) - \alpha \frac{W_{\text{total}}(\tau) - W_{\text{total}}(0)}{W_{\text{total}}(0)} \tag{10}$$

The correction term is included to prevent large fluctuations in the total weight of the walkers.Weights associated with each walker are also updated each time step according to:

$$W_i(\tau + \delta\tau) = \exp\Big[- \big(V_i(\tau + \delta\tau) - E_{\text{ref}}(\tau)\big)\delta\tau\Big] W_i(\tau) \tag{11}$$

In order to maintain a distribution of walkers, walkers with weights below W_{thresh} are replaced. This is accomplished by splitting the highest weight walker into two with half of the weight and removing the low weight walker from the ensemble. In this work, W_{thresh} is defined to be $1/N_{\text{walker}}$. In order to estimate expectation values and construct probability distributions, a technique called descendant weighting is employed.[15] In this scheme, the weight of a walker at a chosen time in the simulation, W_i, as well as the total weight attributed to that original walker after n time steps, $W_i(\tau + n\delta\tau) = D_i$, are used. For an arbitrary multiplicative operator, $\hat{A}$, the expectation value is determined by:

$$\langle A \rangle = \frac{\sum_{i}^{N_{\text{walker}}} W_i A_i D_i}{\sum_{i}^{N_{\text{walker}}} W_i D_i} \tag{12}$$

The values of $W_i D_i$ can also be used to construct a histogram for a given coordinate, which can be interpreted as a probability distribution.

3 Rotational Basis Diffusion Monte Carlo

The calculation of rotationally excited state energies and wavefunctions can be performed with DMC by incorporating a rotational state vector associated with each walker:

$$\langle \vec{R} | \Psi(\tau) \rangle = \sum_{i}^{N_{\text{walker}}} W_i(\tau) \delta^{3N}\big(\vec{R} - \vec{R}_i(\tau)\big) \, |\Phi_{i,J}(\tau)\rangle \tag{13}$$

The state vector $|\Phi_{i,J}\rangle$ utilizes a symmetrized basis of analytic solutions to the symmetric top rigid rotor problem with appropriate coefficients and parity $p = \pm 1$:

$$|\Phi_{i,J}(\tau)\rangle = \sum_{K,p} C_{i,J,K,p}(\tau) \, |J,K\rangle_p \tag{14}$$

$$|J,K\rangle_p = \frac{1}{\sqrt{2p(1+\delta_{K,0})}}[|J,K\rangle + p(-1)^K \, |J,-K\rangle] \tag{15}$$

The coefficients are updated according to first order time-dependent perturbation theory:

$$C_{i,J,K,p}(\tau+\delta\tau) = C_{i,J,K,p}(\tau) - \delta\tau \sum_{K',p} C_{i,J,K',p}(\tau) \, \langle J,K|_p \hat{h}_{\mathrm{rot}}\big(\vec{R}_i(\tau+\delta\tau)\big)|J,K'\rangle_p \tag{16}$$

The states are then orthogonalized by the Gram-Schmidt process and normalized. In these equations, J represents the angular momentum of a basis state and K represents the projection of the angular momentum onto a given axis, the z-axis in this case. The quantum propagator is modified to include a rotational Hamiltonian:

$$\hat{h}_{\mathrm{rot}}(\vec{R}) = \frac{1}{2} \sum_{\alpha,\beta} \hat{J}_\alpha I^{-1}_{\alpha,\beta}(\vec{R}) \hat{J}_\beta \tag{17}$$

$$|\Psi(\tau+\delta\tau)\rangle \approx e^{-(\hat{V}-E_{\mathrm{ref}}(\tau))\delta\tau} e^{-\hat{h}_{\mathrm{rot}}\delta\tau} e^{-\hat{T}\delta\tau} \, |\Psi(\tau)\rangle \tag{18}$$

The α and β in the rotational Hamiltonian are the x, y, and z Cartesian directions, $\hat{J}_\alpha$ is an angular momentum operator, and $I^{-1}_{\alpha,\beta}$ is an element of the inverse moment of inertia tensor. Using the symmetric top basis allows one to use raising and lowering operators to determine the couplings between basis states. Rotational energies are then calculated as expectation values of the rotational Hamiltonian in the Eckart frame:

$$E_{\mathrm{rot}}\big(\vec{R}_i(\tau)\big) = \langle \Phi_{i,J}(\tau)|\hat{h}_{\mathrm{rot}}\big(\vec{R}_i(\tau)\big)|\Phi_{i,J}(\tau)\rangle \tag{19}$$

The Eckart frame is a body fixed coordinate system which minimizes the rotation-vibration coupling. This frame requires a reference geometry, which has been chosen to be the equilibrium geometry. The transformation from the space fixed coordinate system to the

Eckart frame is outlined elsewhere.[16] The resultant rotational energies are added to the walker potential energies prior to calculating a series of reference energies. The principles used to calculate the energies and wavefunctions of rotational states corresponding to a single J value can easily be expanded to include multiple J states in a single calculation.[12] Rather than dressing the walkers with a single rotational state vector, they are dressed with N_{state} vectors, each having a unique weight:

$$\langle \vec{R}|\Psi(\tau)\rangle = \sum_{i=1}^{N_{\text{walker}}} \delta^{3N}\big(\vec{R} - \vec{R}_i(\tau)\big) \begin{pmatrix} W_i^{(1)}(\tau)\,|\Phi_{i,J}^{(1)}(\tau)\rangle \\ W_i^{(2)}(\tau)\,|\Phi_{i,J}^{(2)}(\tau)\rangle \\ W_i^{(3)}(\tau)\,|\Phi_{i,J}^{(3)}(\tau)\rangle \\ \vdots \\ W_i^{(N_{\text{state}})}(\tau)\,|\Phi_{i,J}^{(N_{\text{state}})}(\tau)\rangle \end{pmatrix} \tag{20}$$

The single reference energy is replaced by a vector of length N_{state}. The reference energies and weights are calculated individually as before. This simultaneous calculation of multiple states is a marked difference from previous DMC calculations performed in the McCoy group, where a single state was calculated in each simulation.

3.1 Application to CH_5^+ and its Deuterated Isotopologues

One advantage of the DMC method is its ability to determine the projection of the wavefunction along any number of relevant coordinates. In this section, DMC is used to compare the C-H and H-H bond lengths in $CH_5^+$and its deuterated isotopologues, CH_4D^+, $CH_3D_2^+$, $CH_2D_3^+$, CHD_4^+, and CD_5^+. Rotationally excited states up to $J = 10$ were included in the analysis; the calculated energies for CH_5^+ are given in Table 1. As can be seen in the table, as J increases, the amount of parity mixing in the calculation also increases. Nevertheless, the calculated energies are quite close to rigid rotor energies. For CH_5^+, The variation between energies of K levels for a single J state is observed to be quite small, which is characteristic for a spherical top molecule. This changes for the doubly deuterated isotopologue, which have a greater range of energies. Several of these are included in Table 2. A full tabulation of calculated rotationally excited energies are

given in the Appendix in Table 8. For each isotopologue, a single set of calculations simultaneously produces all of the given energies; this allows correlated sampling to be used in the analysis to minimize the apparent statistical error.

Table 1: Comparison Between the Multi-State DMC and Rigid-Rotor Energies (in cm^{-1}) for Representative Rotationally Excited States of CH_5^+ with 99% confidence intervals

J	$E_{\mathrm{DMC}}^{\mathrm{min},a}$	$\langle p \rangle^b$	$E_{\mathrm{DMC}}^{\mathrm{max},a}$	$\langle p \rangle^b$	$E_{\mathrm{DMC}}^{\mathrm{avg},c}$	$E_{\mathrm{RR}}^{\mathrm{avg},d}$
1	7.70 ± 0.19	1.00	7.77 ± 0.15	1.00	7.75	7.77
2	23.15 ± 0.54	-1.00	23.35 ± 0.47	0.99	23.24	23.24
3	46.35 ± 1.10	0.97	46.62 ± 1.04	-0.94	46.46	46.44
4	77.26 ± 1.77	0.92	77.72 ± 1.33	0.79	77.41	77.37
5	115.71 ± 1.97	0.73	116.46 ± 1.22	-0.67	116.07	116.04
6	161.40 ± 2.87	-0.58	163.04 ± 2.62	0.48	162.40	162.45
7	214.36 ± 4.16	-0.42	217.43 ± 1.39	0.35	216.41	216.59
8	274.58 ± 5.61	0.31	279.73 ± 2.19	-0.22	278.09	278.46
9	342.05 ± 7.27	-0.25	349.50 ± 1.02	0.12	347.43	348.07
10	416.77 ± 9.12	-0.23	427.71 ± 5.85	-0.18	424.46	425.41

[a] The largest and smallest energy evaluated for a given value of J using the multi-state DMC calculations with $J_{\max} = 10$.

[b] The average parity of the DMC state.

[c] The energy average of the calculated $2J + 1$ energies for a given value of J.

[d] Rigid-rotor energies, E_{RR}, are the eigenvalues of the rotational Hamiltonian for the equilibrium structur with averaged rotational constants: $\langle A \rangle_0 = 3.890$ cm^{-1} $\langle B \rangle_0 = 3.862$ cm^{-1} $\langle C \rangle_0 = 3.849$ cm^{-1}

Table 2: Energies of ground and rotationally excited states up to $J = 3$, where $E_{n,method}$ represents the number of deuterium atoms, n, and the method used (DMC or rigid rotor). A full tabulation of rotationally excited energies for CH_5^+ and its deuterated isotopologues up to $J = 10$ is included in the Appendix in Table 8

J	$E_{0,DMC}$	$E_{0,RR}$	$E_{2,DMC}$	$E_{2,RR}$	$E_{3,DMC}$	$E_{3,RR}$
0	10920 ± 7	—	9699 ± 8	—	9097 ± 10	—
1	7.70 ± 0.19	7.71	5.42 ± 0.09	5.49	4.87 ± 0.05	4.88
1	7.77 ± 0.11	7.76	5.64 ± 0.10	5.74	4.89 ± 0.07	4.94
1	7.77 ± 0.15	7.90	5.88 ± 0.12	6.46	5.00 ± 0.02	5.11
2	23.15 ± 0.54	23.12	16.15 ± 0.21	16.45	14.50 ± 0.16	14.53
2	23.19 ± 0.39	23.12	16.33 ± 0.28	16.51	14.75 ± 0.21	14.58
2	23.20 ± 0.43	23.23	17.17 ± 0.25	16.94	14.83 ± 0.16	14.87
2	23.30 ± 0.42	23.33	17.38 ± 0.30	17.48	14.83 ± 0.14	14.94
2	23.35 ± 0.47	23.56	17.69 ± 0.39	18.65	14.89 ± 0.15	15.17
3	46.35 ± 1.10	46.18	31.73 ± 0.44	32.72	29.03 ± 0.36	28.95
3	46.36 ± 1.07	46.19	31.82 ± 0.53	32.77	29.22 ± 0.24	28.97
3	46.38 ± 0.34	46.40	34.23 ± 0.39	33.61	29.40 ± 0.20	29.52
3	46.42 ± 0.85	46.44	34.39 ± 0.64	33.93	29.57 ± 0.36	29.59
3	46.54 ± 0.79	46.51	34.65 ± 0.56	34.18	29.60 ± 0.42	29.85
3	46.59 ± 0.44	46.69	34.86 ± 0.52	35.18	29.91 ± 0.36	29.93
3	46.62 ± 1.04	47.02	35.46 ± 0.86	36.82	29.91 ± 0.36	30.22

As part of the analysis, positions of the hydrogen atoms were assigned to letters, as shown in Figure 2. Positions A and B are given to the two hydrogen atoms that are closest together; these two atoms compose what can be considered an H_2 subunit. Positions B and C are defined by having the next shortest H-H bond length. Positions D and E are given to the remaining hydrogen atoms. An H_3 subunit is composed of the C, D, and E hydrogen atoms; the C-H bonds of these atoms are shorter than those of the H_2 subunit, shown in Figure 3.

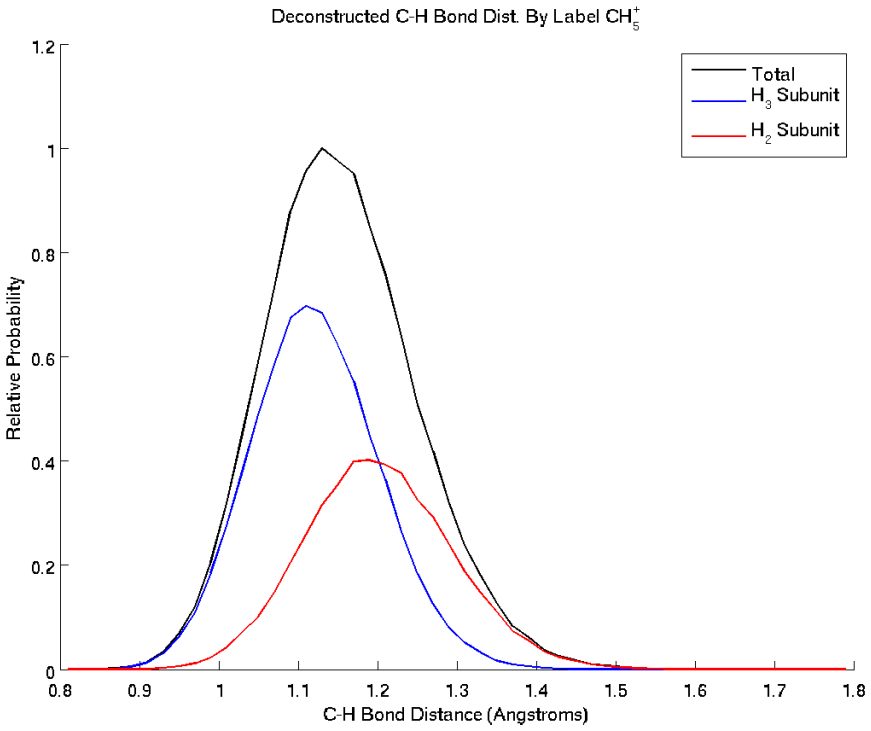

Figure 3: Using the position labels, the hydrogen atoms can be grouped into H_2 and H_3 subunits which have different C-H bond lengths

The analysis of hydrogens based on them being contained in well-defined subunits can also be justified with the probability distribution of the H-H bond lengths. Figure 4b shows the H-H bond lengths in CH_5^+, with a significant shoulder at $r = 1.0$ Å for the H_2 subunit.

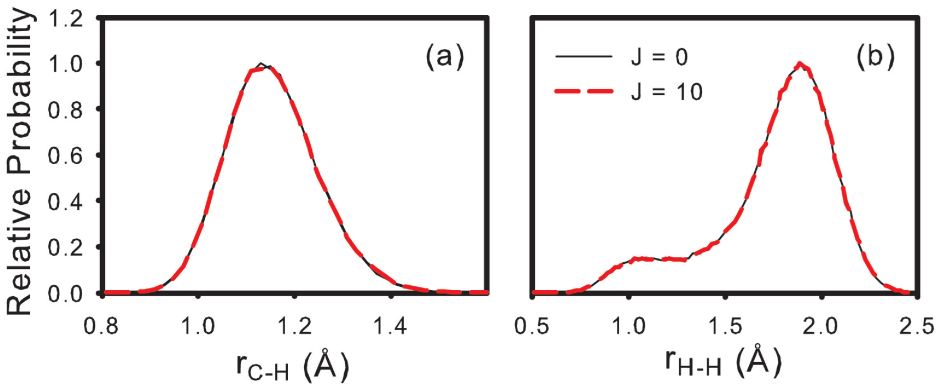

Figure 4: The C-H bond lengths of CH_5^+ nearly compose a normal distribution while the H-H bond lengths have a significant shoulder at shorter bond lengths, representing the H_2 subunit. Analysis of rotationally excited states up to $J = 10$ using DMC shows negligible change in the probability distribution with respect to rotational excitation.

Intuitively, the deuterium atoms tend to localize in the H_3 subunit, as can be seen in Table 3 and in Figure 5. For example, CH_4D^+ was found to have its deuterium atom

in the A or B positions only 7% of the time, while CHD_4^+had its hydrogen atom in A or B 89% of the time. This would be predicted by a simple harmonic oscillator model, due to the heightened mass of the deuterium atom lending itself to a shorter C-H bond length. These results are very similar to previously established results.[13] With rotational excitation up to $J = 10$ in this model, no significant difference was observed.

ABC	% CH_4D^+	% $CH_3D_2^+$	% $CH_2D_3^+$	% CHD_4^+
HHH	75	42	—	—
HHD	18	39	64	—
HDH	2	4	< 1	—
DHH	5	12	24	—
HDD	—	1	09	35
DHD	—	< 1	< 1	54
DDH	—	< 1	1	8
DDD	—	—	< 1	3

Table 3: ABC positions occupied by hydrogen or deuterium atoms; deuterium atoms tend to localize to the C, D, and E positions

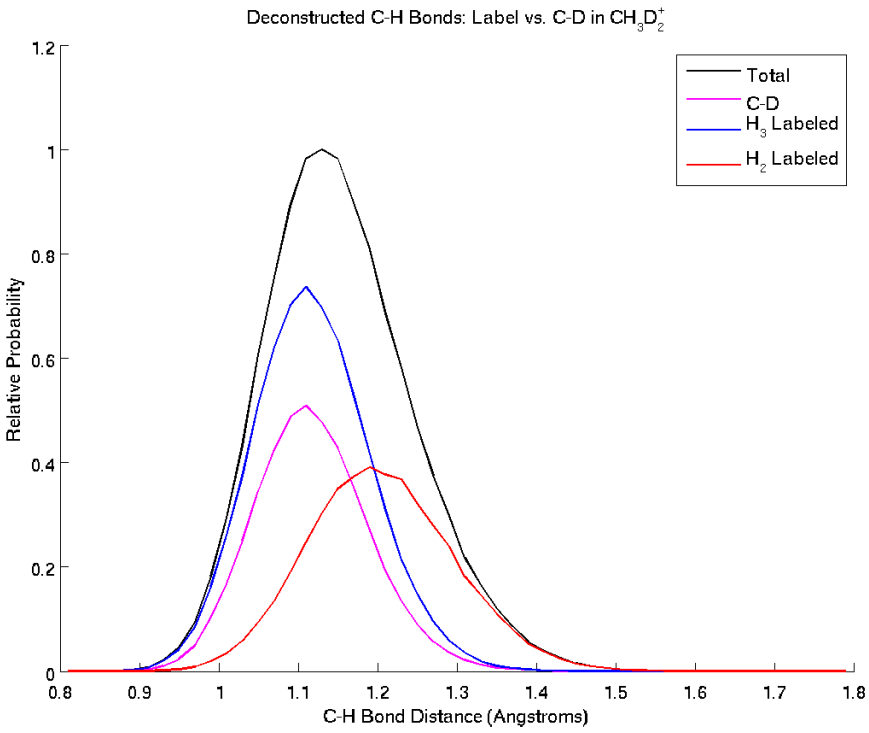

Figure 5: The probability distribution of the C-H/D bonds can be deconstructed for $CH_3D_2^+$ to show that deuterium atoms localize closer to the central carbon atom

Using the position labels, two additional coordinates may be defined, ϕ and q. The coordinate q is determined by the bond lengths between H_A, H_B, H_C:

$$q = r_{BC} - r_{AB} \tag{21}$$

ϕ is determined by first defining the vector connecting the carbon atom to the center of mass of the H_3 subunit to lie along the z-axis. The x-axis is then defined by $\vec{r}_{AB}$ lying in the xz plane. ϕ is then given by the angle between xz plane and the planes containing H_C, H_D, or H_E and the z-axis. Depictions of these two coordinates are given in Figure 6, along with probability distributions for $J = 0$ and $J = 10$. These probability distributions show the hallmark of CH_5^+: all of the hydrogen atoms can permute positions with one another as there is significant probability where $q = 0$ and for all values of ϕ. Again, it is seen that rotational excitation of CH_5^+ within the framework of DMC has negligible effect on the probability distribution. This is not completely unforeseen, as the coupling effects are not explicitly included in the DMC model.

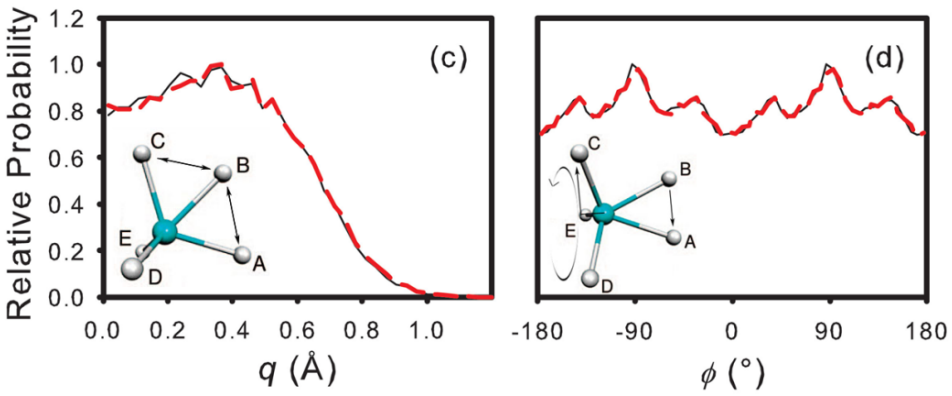

Figure 6: The coordinates q and ϕ are shown above with their respective probability distributions at $J = 0$ (black) and $J = 10$ (dashed red)

Similar plots can be made with respect to deuteration; C-H and H-H bond length distributions, as well as distributions of q and ϕ can be seen below for the doubly and triply deuterated isotopologues in Figures 7 through 10. The presented isotopologues were chosen as they differ the greatest in structure from CH_5^+ due to deuteron/mass localization. As can be seen, the C-H/D and H/D-H/D bond distributions become slightly more localized around 1.1 and 1.9 Å, respectively, with more deuteration. The q coordinate appears to have negligible differences with deuteration, while the ϕ coordinate seems to differ in a complex fashion.

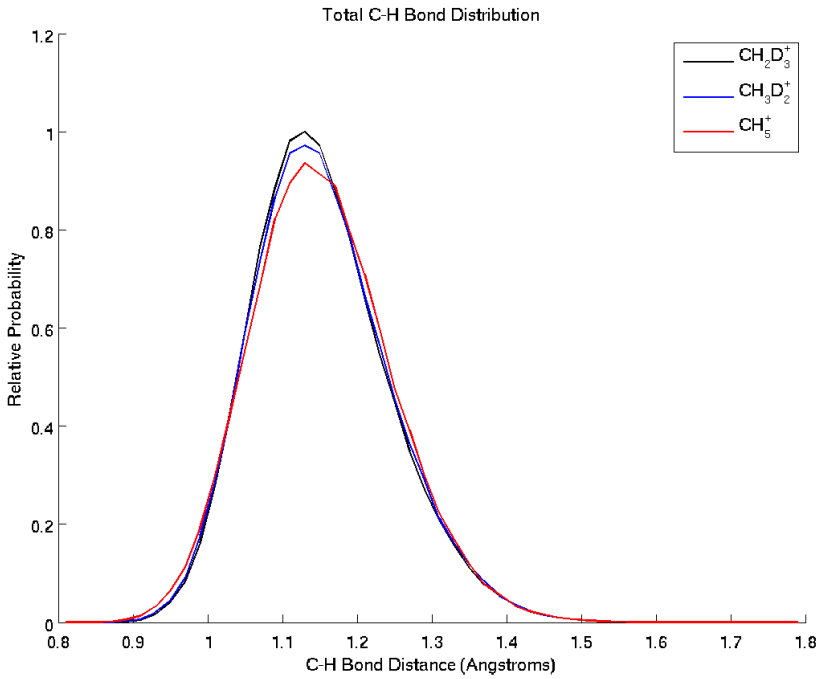

Figure 7: With increasing number of deuterons, the C-H bond length probability distribution tends to localize around 1.1 Å

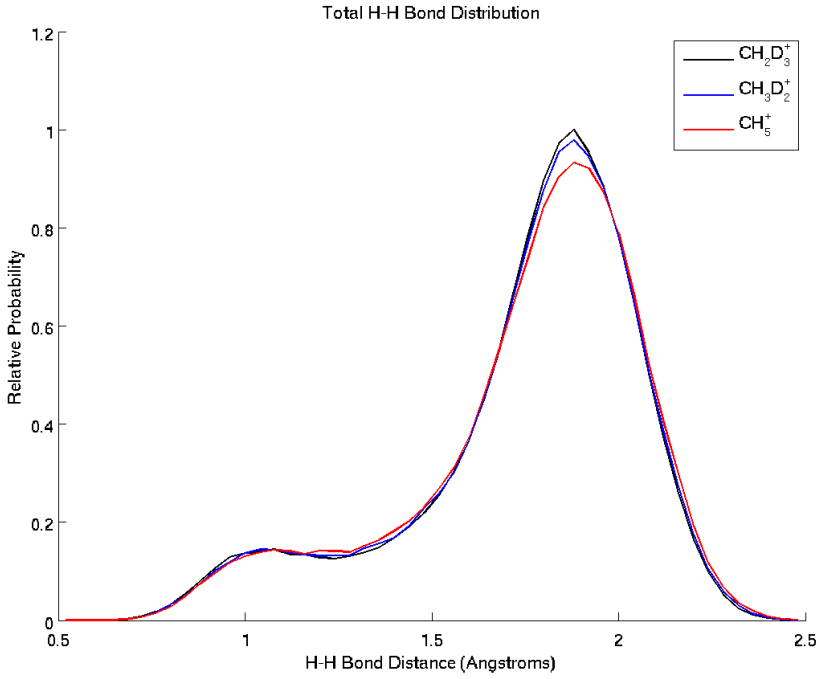

Figure 8: With increasing number of deuterons, the H-H bond length probability distribution tends to localize around 1.9 Å

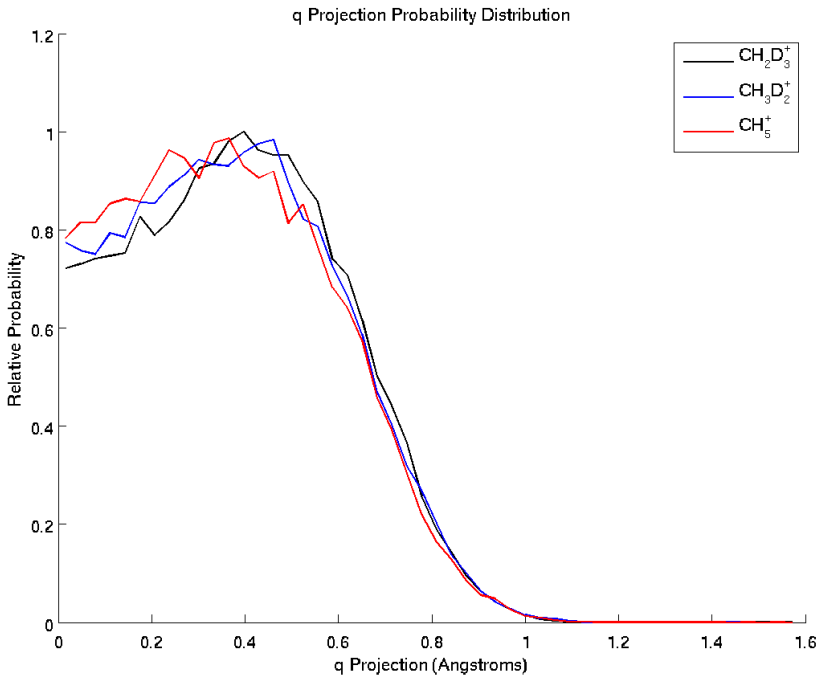

Figure 9: Very little change is observed in q as CH_5^+ is deuterated

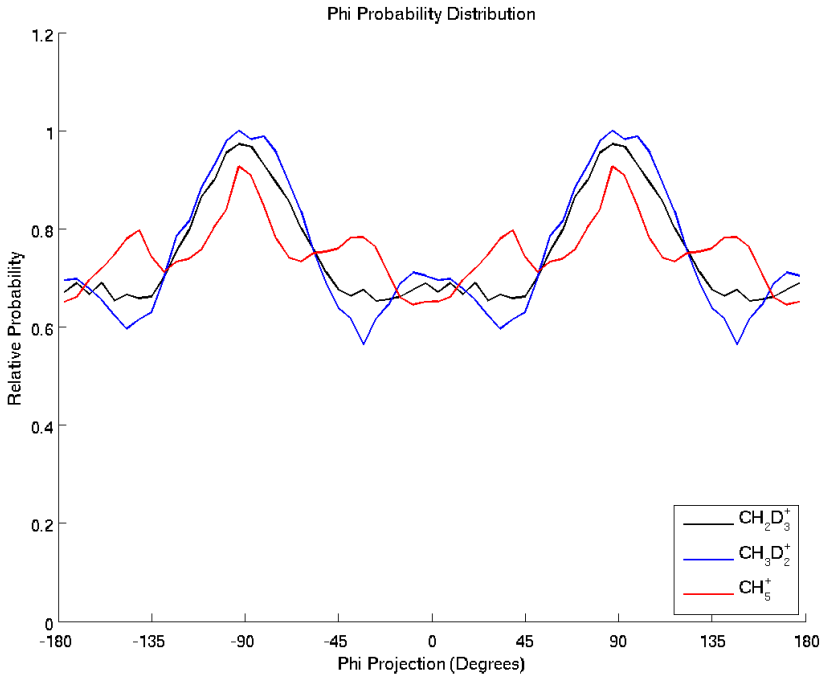

Figure 10: The ϕ coordinate changes in a complex manner as CH_5^+ is deuterated

4 Fixed Node DMC

Vibrations may be incorporated into the DMC calculation by placing a node in the wavefunction.[17,18] In cases with high symmetry, such as the asymmetric stretch of H_2D^+ or HD_2^+, the node may be known analytically. In other cases, the node may be moved adiabatically along a carefully selected coordinate. When the energy is minimized and equal on both sides of the node, the location of the node is optimal.[19] The node is implemented by reducing the weight of a walker to zero if it crosses the node.

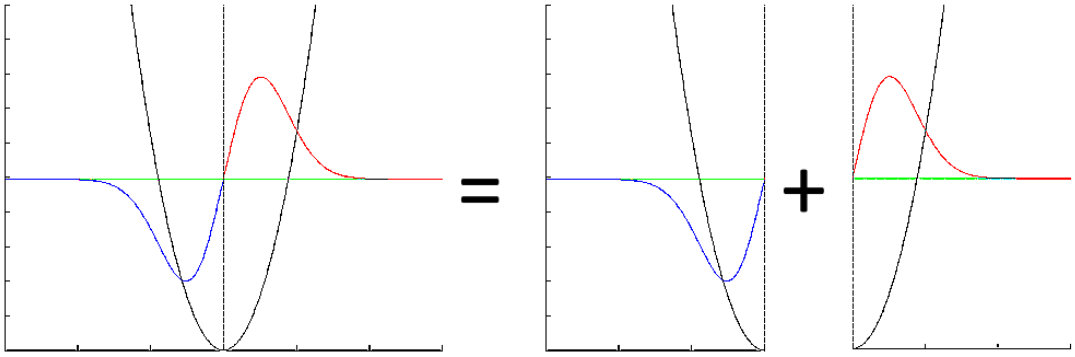

Figure 11: The wavefunction is split into two parts where the amplitude of the wavefunction is zero, such as the equilibrium bond length for the first excited state of a harmonic oscillator

4.1 Recrossing Correction

Due to the finite time step used, there is a nonzero probability that a walker will diffuse across the node and back within a single step. This can largely be overcome by introducing a recrossing correction, as shown by Anderson.[20] The probability that the walker has recrossed the node, P_{recross} as shown in Equation 22, is compared to a random real number, r, in the range (0,1). The walker has its weight set to zero if P_{recross} is greater than r.

$$P_{\text{recross}} = \exp\left[-\frac{m_{\text{eff}} d(\tau) d(\tau+\delta\tau)}{\delta\tau}\right] \tag{22}$$

$$\frac{1}{m_{\text{eff}}} = \sqrt{G^{(s)}_{k,k}(\tau) G^{(s)}_{k,k}(\tau+\delta\tau)} \tag{23}$$

In these equations, m_{eff} is the effective mass for a specific vibrational mode, while $d(\tau)$ is the distance to that node at time τ. The definition of the effective mass requires the use of the diagonal elements of the G-matrix expressed in terms of the nodal coordinates, the background of which is given elsewhere.[21,22] For the asymmetric stretch of H_2D^+, the distance to the node and the effective mass are defined below; the coordinates r_1, r_2, and θ_{HDH} are given in Figure 12.

$$d(\tau) = \frac{1}{\sqrt{2}}\big(r_1(\tau) - r_2(\tau)\big) \tag{24}$$

$$m_{\text{eff}} = \frac{m_{\text{D}} m_{\text{H}}}{\sqrt{\Big(m_{\text{D}} + m_{\text{H}}\big(1 - \cos\theta_{\text{HDH}}(\tau)\big)\Big)\Big(m_{\text{D}} + m_{\text{H}}\big(1 - \cos\theta_{\text{HDH}}(\tau + \delta\tau)\big)\Big)}} \tag{25}$$

5 Rovibrational Excitation in H_2D^+

H_2D^+ provides a highly symmetric test case to determine whether ro-vibrational excitation can be calculated by combining the previously described DMC approaches. The rovibrational state energies have been well characterized by Tennyson et al.[23] The asymmetric stretch of H_2D^+, corresponding to the nuclear motions in Figure 12, has an analytically known node when the two H-D bond lengths are equal in length. Using the rotational basis and fixed node methods synchronously provides the sets of energies for the H_2D^+ rovibrational energies given in Table 4. Just like the CH_5^+ calculations earlier, all energies are found simultaneously in a single set of calculations, allowing one to use correlated sampling to reduce the statistical error. It should be noted here that the DMC method was altered to "symmetrize" the walkers. The walkers are given weights for both the ground and vibrationally excited state. The geometry of walkers was flipped if they crossed the asymmetric stretch node, therefore forcing a constant sign of the $I_{xy}^{-1}(J_xJ_y + J_yJ_x)$ coupling term. This term coupled the ground and vibrationally excited states in the rotational Hamiltonian. As can be seen in the table, the $\nu_{\text{asym}} = 0$ energies are quite accurate, while the rotationally excited $\nu_{\text{asym}} = 1$ energies differ by up to 20 cm^{-1}. An identical trend is seen in Table 5 for the analogous HD_2^+ ion.

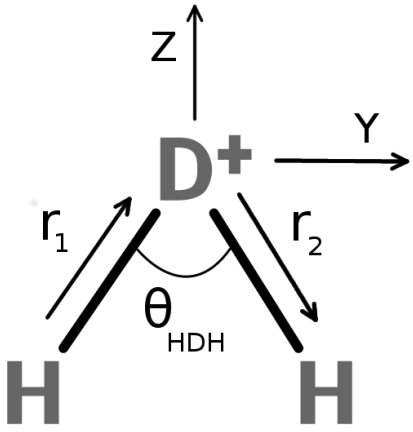

Figure 12: H_2D^+ is shown with arrows representing the asymmetric stretch, as well as the definitions for the axes

Table 4: H_2D^+ Rovibrational Energies

Rot. State $\|J,K\rangle_p$ − ZPE	$\nu = 0$ DMC Energy (cm^{-1})	$\nu = 0$ Var. Energy (cm^{-1})[23]	$\nu = 1$ DMC Energy (cm^{-1})	$\nu = 1$ Var. Energy (cm^{-1})[23]
$\|0,0\rangle$	3978 ± 9	—	2333 ± 6	2335.0
$\|1,1\rangle_+$	45.6 ± 0.3	45.7	43.2 ± 0.4	48.5
$\|1,1\rangle_-$	59.8 ± 0.2	60.0	61.6 ± 0.7	67.4
$\|1,0\rangle_+$	72.5 ± 0.2	72.4	73.9 ± 0.7	73.9
$\|2,2\rangle_+$	131.2 ± 1.1	131.6	125.1 ± 0.9	142.3
$\|2,2\rangle_-$	138.1 ± 0.5	138.8	135.8 ± 1.2	155.6
$\|2,1\rangle_+$	176.1 ± 1.1	175.9	172.6 ± 1.5	177.0
$\|2,1\rangle_-$	218.5 ± 0.7	218.6	227.8 ± 2.4	233.0
$\|2,0\rangle_+$	223.9 ± 0.9	223.8	232.1 ± 2.7	234.1

Table 5: HD_2^+ Rovibrational Energies

Rot. State $\|J,K\rangle_p$ − ZPE	$\nu = 0$ DMC Energy (cm^{-1})	$\nu = 0$ Var. Energy (cm^{-1})[23]	$\nu = 1$ DMC Energy (cm^{-1})	$\nu = 1$ Var. Energy (cm^{-1})[23]
$\|0,0\rangle$	3563 ± 6	—	2081 ± 8	2079.2
$\|1,1\rangle_+$	34.7 ± 0.2	34.9	35.3 ± 0.3	40.1
$\|1,1\rangle_-$	49.1 ± 0.3	49.2	47.3 ± 0.9	50.2
$\|1,0\rangle_+$	57.9 ± 0.3	58.0	57.7 ± 0.8	57.8
$\|2,2\rangle_+$	101.8 ± 0.8	101.7	102.2 ± 1.2	115.4
$\|2,2\rangle_-$	109.6 ± 0.5	110.2	107.7 ± 1.1	124.1
$\|2,1\rangle_+$	136.2 ± 0.6	136.3	138.8 ± 1.3	146.5
$\|2,1\rangle_-$	179.1 ± 1.1	179.1	174.6 ± 3.2	176.2
$\|2,0\rangle_+$	181.5 ± 1.0	182.0	178.3 ± 3.3	179.1

5.1 Group Theoretical Analysis

Using group theory, one can gain an understanding of the failure of the calculation. The mixing of states of the same symmetry, namely Coriolis coupling, is not explicitly included in the DMC calculation, and the resultant energies therefore differ. Coriolis coupling terms require nontrivial calculation and do not present an obvious extension to the current DMC method. Rotational excitation is determined by rotations of the space fixed coordinate frame into the body fixed Eckart frame by Euler angles. As stated before, the Eckart frame is used as it has been shown to minimize the coupling between rotations and vibrations. Euler angles, as shown in Figure 13, can have many different conventions, but generally, a rotation from one coordinate frame to another in 3-dimensional space requires 3 angles, χ, θ, and ϕ. The functions used to describe rotational excitation, and their irreducible representations, are given below in Table 6.

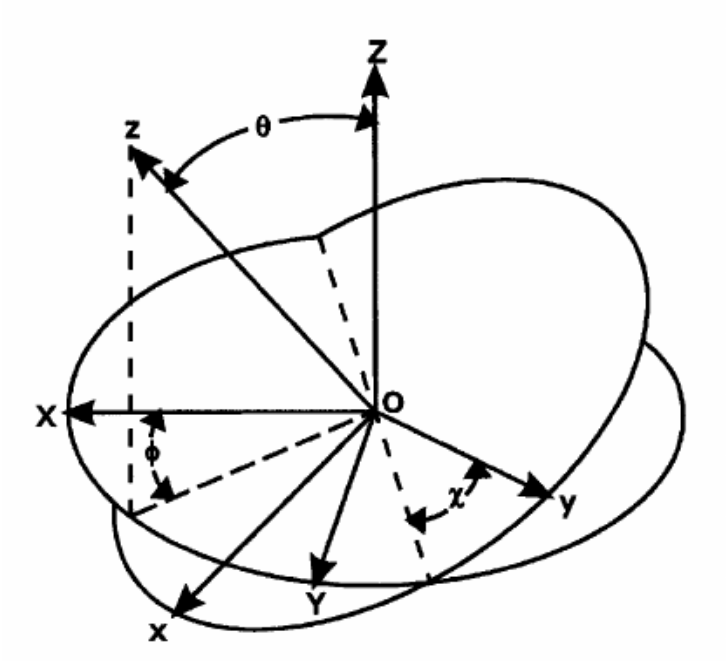

Figure 13: Rotational excitation is defined by functions of the Euler angles depicted here

C_{2v}	E	C_2	σ_{xz}	σ_{yz}	Γ
A_1	1	1	1	1	–
A_2	1	1	-1	-1	–
B_1	1	-1	1	-1	–
B_2	1	-1	-1	1	–
θ	θ	$\pi-\theta$	θ	$\pi-\theta$	–
χ	χ	$-\chi$	$-\chi$	χ	–
$\|1,1\rangle_+ \propto \sin\theta\cos\chi$	1	1	1	1	A_1
$\|1,1\rangle_- \propto \sin\theta\sin\chi$	1	-1	-1	1	B_2
$\|1,0\rangle_+ \propto \cos\theta$	1	-1	1	-1	B_1
$\|2,2\rangle_+ \propto \sin^2\theta\cos 2\chi$	1	1	1	1	A_1
$\|2,2\rangle_- \propto \sin^2\theta\sin 2\chi$	1	-1	-1	1	B_2
$\|2,1\rangle_+ \propto \sin\theta\cos\theta\cos\chi$	1	-1	1	-1	B_1
$\|2,1\rangle_- \propto \sin\theta\cos\theta\sin\chi$	1	1	-1	-1	A_2
$\|2,0\rangle_+ \propto 3\cos^2\theta-1$	1	1	1	1	A_1

Table 6: Character table for the C_{2v} point group, in which H_2D^+ belongs, including the symmetrized rotational basis functions.

Taking the direct product of irreducible representations of rotationally excited states with that of vibrationally excited states gives a final irreducible representation of calculated states. These can then be compared between states that have one quantum of excitation in the asymmetric stretch versus those that have one in the bend vibration, the nearest set of energy levels. The final irreducible representations, as well as state energies, are given below for $J = 0, 1, 2$ and $\nu = 1$ in the bend and asymmetric stretch in Table 7.

State $\|J,K\rangle_p$	Bend Irr. Rep.	Bend Rovib. Energy (cm^{-1})	Asym. Str. Irr. Rep.	DMC Asym. Str. Energy (cm^{-1})	Var.-DMC Rovib. Energy (cm^{-1})
$\|0,0\rangle$	A_1	2206.244	B_2	2333.4	1.6
$\|1,1\rangle_+$	A_1	2247.018	B_2	2376.6	5.4
$\|1,1\rangle_-$	B_2	2259.132	A_1	2395.0	5.7
$\|1,0\rangle_+$	B_1	2278.765	A_2	2407.3	-0.1
$\|2,2\rangle_+$	A_1	2318.616	B_2	2458.5	17.2
$\|2,2\rangle_-$	B_2	2322.992	A_1	2469.2	19.8
$\|2,1\rangle_+$	B_1	2379.618	A_2	2506.0	4.4
$\|2,1\rangle_-$	A_2	2415.760	B_1	2561.2	5.3
$\|2,0\rangle_+$	A_1	2427.370	B_2	2565.5	2.0

Table 7: Listing of irreducible representations of rovibrational states of H_2D^+, as well as comparison of DMC to variationally calculated literature values and the energy gaps between states of the same symmetry

Using the energy gaps and irreducible representation labels, an energy level diagram can be constructed showing the mixing that is occuring versus what is being calculated. This

has been done for the $J = 1$ states below, showing that if mixing between bend excited and asymmetric stretch excited states was included, the energy levels of the asymmetric stretch states would be pushed upward.

Figure 14: The following energy level diagram shows how the mixing of excluded states from the DMC calculation likely lead to the error in the calculation

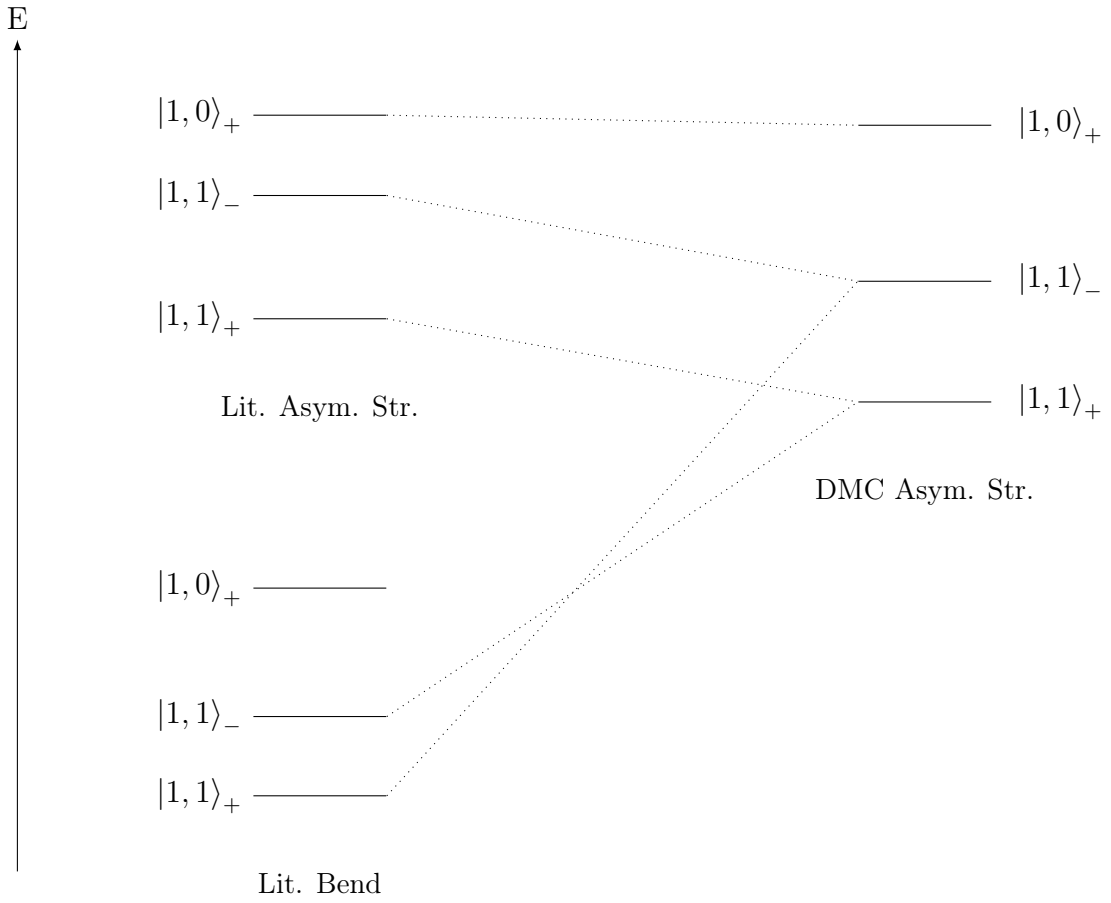

6 Conclusion

In this work, we have provided an advancement in diffusion Monte Carlo methodology, allowing quick application to rotationally excited states of small molecules. This was used to show that rotational excitation of CH_5^+ and its deuterated isotopologues has little effect on the overall wavefunction. It was also used to increase the body of evidence that hydrogen and deuterium atoms will tend to localize in a predictable manner around the central carbon atom in these molecules. The methodology was then tested with fixed node diffusion Monte Carlo, to determine the efficacy of combining the approaches for

rovibrational effects. The combined method had significantly larger errors, which was shown to likely occur from the exclusion of Coriolis coupling terms. These terms present a nontrivial addition to diffusion Monte Carlo methodology for further testing.

7 Acknowledgement

I personally thank the McCoy research group for their continued support. I also sincerely thank the College of Arts and Sciences and the Division of Natural and Mathematical Sciences at Ohio State for generous financial support through the Undergraduate Research Scholarship and the Mayers Summer Research Scholarship, respectively. Lastly, I thank the NSF for funding and the Ohio Supercomputer Center for computing resources.

References

[1] Bernath, P. *Spectra of Atoms and Molecules*; Oxford University Press, USA, 2005.

[2] Herbst, E. *Annual Review of Physical Chemistry* **1995**, *46*, 27–54.

[3] Relph, R. A.; Guasco, T. L.; Elliott, B. M.; Kamrath, M. Z.; McCoy, A. B.; Steele, R. P.; Schofield, D. P.; Jordan, K. D.; Viggiano, A. A.; Ferguson, E. E.; Johnson, M. A. *Science* **2010**, *327*, 308–312.

[4] Liu, F.; Beames, J. M.; Petit, A. S.; McCoy, A. B.; Lester, M. I. *Science* **2014**, *345*, 1596–1598.

[5] White, E. T.; Tang, J.; Oka, T. *Science* **1999**, *284*, 135–137.

[6] Wang, X.-G.; Carrington, T. *The Journal of Chemical Physics* **2008**, *129*, –.

[7] Rapisarda, F.; Senatore, G. *Australian journal of physics* **1996**, *49*, 161–182.

[8] Pederiva, F.; Umrigar, C.; Lipparini, E. *Physical Review B* **2000**, *62*, 8120.

[9] Giorgini, S.; Boronat, J.; Casulleras, J. *Physical Review A* **1999**, *60*, 5129.

[10] Sun, H.; Watts, R. O. *The Journal of Chemical Physics* **1990**, *92*.

[11] Liu, K.; Brown, M.; Carter, C.; Saykally, R.; Gregory, J.; Clary, D. *Nature* **1996**, *381*, 501–503.

[12] Petit, A. S.; Ford, J. E.; McCoy, A. B. *The Journal of Physical Chemistry A* **2014**, *118*, 7206–7220, PMID: 24053598.

[13] Johnson, L. M.; McCoy, A. B. *The Journal of Physical Chemistry A* **2006**, *110*, 8213–8220, PMID: 16805509.

[14] Anderson, J. B. *The Journal of Chemical Physics* **1975**, *63*, 1499–1503.

[15] Suhm, M. A.; Watts, R. O. *Physics Reports* **1991**, *204*, 293 – 329.

[16] Louck, J. D.; Galbraith, H. W. *Rev. Mod. Phys.* **1976**, *48*, 69–106.

[17] Ceperley, D. M.; Alder, B. J. *Phys. Rev. Lett.* **1980**, *45*, 566–569.

[18] Reynolds, P. J.; Ceperley, D. M.; Alder, B. J.; Lester, W. A. *The Journal of Chemical Physics* **1982**, *77*.

[19] Lee, H.-S.; Herbert, J. M.; McCoy, A. B. *The Journal of Chemical Physics* **1999**, *110*.

[20] Anderson, J. B. *The Journal of Chemical Physics* **1976**, *65*, 4121–4127.

[21] Wilson, E.; Decius, J.; Cross, P. *Molecular Vibrations: The Theory of Infrared and Raman Vibrational Spectra*; Dover Books on Chemistry; Dover Publications, 2012.

[22] Petit, A. *OhioLINK Electronic Theses and Dissertations Center* **2013**,

[23] Miller, S.; Tennyson, J.; Sutcliffe, B. T. *Molecular Physics* **1989**, *66*, 429–456.

8 Appendix

Table 8: Tabulation of rotationally excited energies in cm^{-1} with 99% confidence intervals for CH_5^+ and its deuterated isotopologues, calculated by rotational basis DMC; the given $J = 0$ energies correspond to calculated zero point energies

J	CH_5^+	CH_4D^+	$CH_3D_2^+$	$CH_2D_3^+$	CHD_4^+	CD_5^+
0	10920 ± 7	10303 ± 4	9699 ± 8	9097 ± 10	8567 ± 7	8042 ± 5
1	7.70 ± 0.19	6.23 ± 0.06	5.42 ± 0.09	4.87 ± 0.05	4.34 ± 0.07	3.90 ± 0.07
1	7.77 ± 0.11	6.76 ± 0.08	5.64 ± 0.10	4.89 ± 0.07	4.34 ± 0.08	3.94 ± 0.05
1	7.77 ± 0.15	6.77 ± 0.10	5.88 ± 0.12	5.00 ± 0.02	4.37 ± 0.08	3.95 ± 0.10
2	23.15 ± 0.54	18.70 ± 0.17	16.15 ± 0.21	14.50 ± 0.16	12.97 ± 0.19	11.73 ± 0.26
2	23.19 ± 0.39	19.16 ± 0.10	16.33 ± 0.28	14.75 ± 0.21	12.99 ± 0.22	11.74 ± 0.18
2	23.20 ± 0.43	19.17 ± 0.22	17.17 ± 0.25	14.83 ± 0.16	13.09 ± 0.22	11.75 ± 0.24
2	23.30 ± 0.42	20.89 ± 0.38	17.38 ± 0.30	14.83 ± 0.14	13.09 ± 0.29	11.81 ± 0.28
2	23.35 ± 0.47	20.89 ± 0.38	17.69 ± 0.39	14.89 ± 0.15	13.11 ± 0.28	11.88 ± 0.22
3	46.35 ± 1.10	37.39 ± 0.33	31.73 ± 0.44	29.03 ± 0.36	25.89 ± 0.50	23.46 ± 0.61
3	46.36 ± 1.07	37.75 ± 0.48	31.82 ± 0.53	29.22 ± 0.24	25.90 ± 0.50	23.46 ± 0.61
3	46.38 ± 0.34	37.77 ± 0.32	34.23 ± 0.39	29.40 ± 0.20	26.09 ± 0.11	23.48 ± 0.46
3	46.42 ± 0.85	39.43 ± 0.24	34.39 ± 0.64	29.57 ± 0.36	26.14 ± 0.40	23.54 ± 0.54
3	46.54 ± 0.79	39.45 ± 0.25	34.65 ± 0.56	29.60 ± 0.42	26.19 ± 0.41	23.58 ± 0.22
3	46.59 ± 0.44	42.42 ± 0.90	34.86 ± 0.52	29.91 ± 0.36	26.23 ± 0.72	23.68 ± 0.26
3	46.62 ± 1.04	42.42 ± 0.90	35.46 ± 0.86	29.91 ± 0.36	26.24 ± 0.71	23.75 ± 0.51
4	77.26 ± 1.77	62.30 ± 0.57	52.28 ± 0.73	48.44 ± 0.49	43.07 ± 0.93	39.07 ± 0.86
4	77.26 ± 1.75	62.49 ± 0.82	52.30 ± 0.80	48.56 ± 0.65	43.07 ± 0.93	39.08 ± 1.10
4	77.29 ± 0.56	62.61 ± 0.65	55.59 ± 0.54	48.64 ± 0.45	43.40 ± 0.39	39.08 ± 1.11
4	77.37 ± 1.39	64.13 ± 0.20	55.72 ± 0.94	49.19 ± 0.67	43.45 ± 0.50	39.11 ± 0.92
4	77.38 ± 1.30	64.20 ± 0.47	57.93 ± 0.95	49.20 ± 0.35	43.59 ± 0.36	39.31 ± 0.46
4	77.44 ± 0.55	67.15 ± 0.68	58.15 ± 1.26	49.23 ± 0.33	43.63 ± 0.80	39.34 ± 0.48
4	77.47 ± 1.67	67.15 ± 0.68	58.53 ± 0.86	49.34 ± 0.69	43.65 ± 0.58	39.34 ± 0.45
4	77.53 ± 0.48	71.35 ± 1.63	58.69 ± 0.91	50.08 ± 0.64	43.76 ± 1.38	39.52 ± 0.86
4	77.72 ± 1.33	71.35 ± 1.63	58.74 ± 1.48	50.08 ± 0.64	43.76 ± 1.38	39.56 ± 0.67
5	115.71 ± 1.97	93.38 ± 0.97	77.80 ± 1.02	72.59 ± 0.81	64.49 ± 1.49	58.52 ± 1.41
5	115.77 ± 2.31	93.38 ± 1.18	77.81 ± 1.07	72.62 ± 0.82	64.49 ± 1.49	58.54 ± 1.44
5	115.87 ± 1.15	93.72 ± 1.09	81.94 ± 0.86	73.16 ± 0.97	64.98 ± 0.78	58.62 ± 1.71
5	115.89 ± 2.31	95.00 ± 0.42	81.98 ± 1.28	73.22 ± 0.50	65.00 ± 0.79	58.62 ± 1.72
5	115.89 ± 2.31	95.10 ± 1.01	85.44 ± 1.64	73.27 ± 0.58	65.27 ± 0.54	58.92 ± 0.87
5	115.98 ± 1.84	98.04 ± 0.54	85.74 ± 1.12	73.64 ± 1.09	65.36 ± 1.02	58.93 ± 0.89
5	116.21 ± 0.59	98.05 ± 0.56	87.06 ± 2.19	73.84 ± 1.04	65.43 ± 1.19	58.96 ± 0.87
5	116.23 ± 0.93	102.25 ± 1.35	87.59 ± 1.56	74.30 ± 0.54	65.48 ± 0.89	59.09 ± 0.64
5	116.25 ± 0.96	102.25 ± 1.35	87.94 ± 1.83	74.30 ± 0.54	65.48 ± 0.82	59.10 ± 1.23
5	116.46 ± 2.20	107.67 ± 2.57	88.18 ± 1.38	75.37 ± 1.00	65.68 ± 2.25	59.19 ± 0.67
5	116.46 ± 1.22	107.67 ± 2.57	89.18 ± 1.25	75.37 ± 1.00	65.68 ± 2.25	59.35 ± 1.17
6	161.40 ± 2.87	130.42 ± 1.62	108.30 ± 1.34	101.49 ± 1.36	90.13 ± 2.19	81.81 ± 2.11

Continued on next page

Table 8 – continued from previous page

J	CH_5^+	CH_4D^+	$CH_3D_2^+$	$CH_2D_3^+$	CHD_4^+	CD_5^+
6	161.42 ± 3.07	130.58 ± 1.57	108.30 ± 1.31	101.67 ± 0.79	90.13 ± 2.19	81.81 ± 2.13
6	162.08 ± 2.04	131.10 ± 1.62	113.32 ± 1.28	102.00 ± 1.24	90.81 ± 1.31	82.09 ± 2.45
6	162.17 ± 2.20	132.07 ± 0.80	113.35 ± 1.63	102.26 ± 0.96	90.81 ± 1.31	82.09 ± 2.44
6	162.27 ± 2.59	132.14 ± 1.68	117.48 ± 2.01	102.53 ± 1.24	91.25 ± 0.91	82.40 ± 1.36
6	162.28 ± 2.55	135.09 ± 0.62	117.72 ± 1.15	102.81 ± 1.62	91.31 ± 1.07	82.45 ± 1.44
6	162.58 ± 0.86	135.13 ± 0.79	120.71 ± 2.77	102.90 ± 1.51	91.53 ± 0.92	82.46 ± 1.46
6	162.64 ± 2.96	139.32 ± 1.11	120.99 ± 2.82	103.28 ± 0.63	91.56 ± 1.75	82.50 ± 1.64
6	162.71 ± 1.37	139.32 ± 1.11	121.97 ± 1.68	103.34 ± 0.67	91.57 ± 1.45	82.71 ± 0.92
6	162.76 ± 1.30	144.74 ± 2.23	123.83 ± 2.27	104.52 ± 0.83	91.71 ± 1.46	82.74 ± 0.93
6	162.94 ± 0.52	144.74 ± 2.23	123.84 ± 2.27	104.52 ± 0.82	91.75 ± 1.47	82.76 ± 1.03
6	162.97 ± 1.44	151.38 ± 3.75	124.05 ± 2.50	105.77 ± 1.45	91.98 ± 3.32	82.97 ± 1.67
6	163.04 ± 2.62	151.38 ± 3.75	124.87 ± 1.68	105.77 ± 1.45	91.99 ± 3.32	82.98 ± 1.19
7	214.36 ± 4.16	173.58 ± 2.21	143.76 ± 1.66	134.58 ± 1.17	119.98 ± 3.01	108.93 ± 3.01
7	214.37 ± 4.09	173.84 ± 2.35	143.76 ± 1.64	135.64 ± 2.05	119.98 ± 3.01	108.93 ± 3.00
7	215.80 ± 2.67	174.76 ± 2.19	149.73 ± 1.73	136.24 ± 1.56	120.86 ± 1.99	109.52 ± 3.33
7	215.86 ± 3.11	175.32 ± 2.26	149.75 ± 1.99	136.38 ± 2.18	120.86 ± 1.99	109.52 ± 3.34
7	216.18 ± 3.86	175.40 ± 1.38	154.72 ± 2.41	136.39 ± 1.47	121.48 ± 1.32	109.67 ± 1.96
7	216.48 ± 1.31	178.28 ± 0.84	154.77 ± 1.40	136.49 ± 2.27	121.49 ± 1.34	109.71 ± 2.17
7	216.49 ± 2.59	178.34 ± 1.46	158.66 ± 3.19	136.54 ± 1.46	121.87 ± 1.40	109.91 ± 2.12
7	216.49 ± 2.58	182.55 ± 1.07	160.26 ± 2.48	136.87 ± 0.92	121.93 ± 1.92	109.92 ± 2.13
7	216.91 ± 1.59	182.56 ± 1.06	160.32 ± 4.58	137.26 ± 1.00	122.01 ± 2.42	110.21 ± 1.39
7	216.98 ± 1.47	187.97 ± 1.92	162.26 ± 2.71	138.48 ± 0.82	122.08 ± 1.66	110.24 ± 1.48
7	217.03 ± 4.20	187.97 ± 1.92	162.69 ± 2.40	138.53 ± 0.83	122.17 ± 1.43	110.24 ± 1.47
7	217.23 ± 1.16	194.61 ± 3.33	165.74 ± 3.28	139.86 ± 1.19	122.34 ± 2.26	110.38 ± 2.17
7	217.25 ± 2.43	194.61 ± 3.33	166.12 ± 2.98	139.86 ± 1.19	122.41 ± 2.34	110.40 ± 1.28
7	217.32 ± 1.15	202.46 ± 5.16	166.18 ± 2.70	141.28 ± 1.98	122.67 ± 4.55	110.48 ± 1.27
7	217.43 ± 1.39	202.46 ± 5.16	166.21 ± 3.69	141.28 ± 1.98	122.68 ± 4.56	110.64 ± 1.77
8	274.58 ± 5.61	222.85 ± 2.99	184.20 ± 2.06	173.16 ± 2.18	154.02 ± 3.99	139.90 ± 4.12
8	274.60 ± 5.62	223.13 ± 3.26	184.20 ± 2.05	174.21 ± 3.11	154.02 ± 3.99	139.90 ± 4.10
8	276.74 ± 3.64	224.59 ± 2.92	191.12 ± 2.19	174.28 ± 2.13	155.12 ± 2.81	140.75 ± 2.85
8	277.02 ± 5.03	224.64 ± 2.81	191.14 ± 2.36	174.43 ± 3.05	155.12 ± 2.81	140.76 ± 2.69
8	277.16 ± 4.22	225.06 ± 2.19	197.03 ± 2.86	174.74 ± 1.36	155.93 ± 1.92	140.95 ± 4.45
8	277.93 ± 1.99	227.63 ± 1.05	197.03 ± 1.96	174.86 ± 1.33	155.93 ± 1.92	140.95 ± 4.45
8	278.23 ± 5.51	227.65 ± 2.56	201.91 ± 3.55	174.88 ± 2.59	156.50 ± 1.77	141.32 ± 2.86
8	278.67 ± 2.91	231.93 ± 1.39	202.77 ± 2.55	176.03 ± 2.13	156.51 ± 1.90	141.34 ± 2.91
8	278.70 ± 2.87	231.96 ± 1.33	204.53 ± 5.45	176.19 ± 1.47	156.77 ± 3.04	141.50 ± 1.99
8	278.83 ± 3.37	237.36 ± 1.76	207.32 ± 2.99	177.19 ± 1.02	156.78 ± 2.85	141.55 ± 2.68
8	278.88 ± 1.47	237.37 ± 1.75	207.41 ± 3.22	177.46 ± 1.09	156.88 ± 2.14	141.65 ± 2.08
8	278.93 ± 1.37	244.00 ± 2.95	209.09 ± 4.20	178.80 ± 1.08	157.01 ± 2.04	141.69 ± 2.18
8	279.20 ± 2.23	244.00 ± 2.95	209.47 ± 3.63	178.81 ± 1.09	157.21 ± 2.14	141.88 ± 1.56
8	279.31 ± 1.11	251.86 ± 4.67	213.46 ± 4.35	180.30 ± 1.64	157.36 ± 3.26	141.94 ± 1.75
8	279.44 ± 1.24	251.86 ± 4.67	213.51 ± 4.18	180.31 ± 1.64	157.43 ± 3.38	141.95 ± 1.72

Continued on next page

Table 8 – continued from previous page

J	CH_5^+	CH_4D^+	$CH_3D_2^+$	$CH_2D_3^+$	CHD_4^+	CD_5^+
8	279.50 ± 2.18	260.89 ± 6.78	213.79 ± 4.54	181.91 ± 2.59	157.72 ± 5.95	142.10 ± 2.31
8	279.73 ± 2.19	260.89 ± 6.78	213.92 ± 2.94	181.91 ± 2.59	157.72 ± 5.94	142.10 ± 1.77
9	342.05 ± 7.27	278.21 ± 3.99	229.64 ± 2.59	216.38 ± 4.21	192.24 ± 5.12	174.70 ± 5.48
9	342.06 ± 7.31	278.42 ± 4.27	229.64 ± 2.59	216.50 ± 4.01	192.24 ± 5.12	174.70 ± 5.47
9	344.93 ± 5.38	279.98 ± 3.87	237.48 ± 2.69	216.67 ± 1.69	193.57 ± 3.77	175.63 ± 3.73
9	345.13 ± 6.44	280.67 ± 3.54	237.50 ± 2.80	217.04 ± 3.06	193.57 ± 3.77	175.65 ± 3.60
9	345.88 ± 5.23	281.05 ± 3.08	244.32 ± 2.61	217.61 ± 2.71	194.60 ± 2.71	176.41 ± 5.82
9	346.63 ± 6.31	283.14 ± 3.11	244.36 ± 3.31	217.63 ± 2.31	194.60 ± 2.70	176.42 ± 5.82
9	347.00 ± 2.97	283.17 ± 1.34	250.10 ± 3.97	218.55 ± 2.97	195.33 ± 2.17	176.49 ± 3.26
9	347.66 ± 3.80	287.43 ± 1.95	250.54 ± 2.44	220.38 ± 2.09	195.36 ± 2.17	176.55 ± 2.61
9	348.36 ± 3.36	287.51 ± 1.98	254.63 ± 5.75	220.39 ± 1.34	195.75 ± 3.11	176.73 ± 3.74
9	348.64 ± 1.45	292.90 ± 1.92	256.01 ± 3.34	220.51 ± 1.95	195.79 ± 4.03	176.73 ± 3.77
9	348.81 ± 0.98	292.91 ± 1.88	256.18 ± 3.87	221.41 ± 1.58	195.88 ± 2.70	177.04 ± 2.91
9	348.84 ± 1.47	299.53 ± 2.69	259.76 ± 5.07	222.59 ± 1.19	195.95 ± 3.14	177.11 ± 3.05
9	349.04 ± 4.07	299.54 ± 2.69	260.70 ± 5.13	222.67 ± 1.22	196.30 ± 2.96	177.27 ± 2.14
9	349.05 ± 4.04	307.40 ± 4.20	261.90 ± 5.01	224.21 ± 1.44	196.38 ± 2.76	177.29 ± 2.11
9	349.35 ± 3.66	307.40 ± 4.20	262.17 ± 3.79	224.21 ± 1.44	196.61 ± 3.09	177.31 ± 2.73
9	349.36 ± 2.03	316.46 ± 6.22	266.19 ± 5.01	225.86 ± 2.18	196.76 ± 4.44	177.36 ± 2.43
9	349.38 ± 2.38	316.46 ± 6.22	266.65 ± 5.60	225.86 ± 2.18	196.80 ± 4.53	177.42 ± 1.88
9	349.44 ± 2.41	326.63 ± 8.54	267.16 ± 4.49	227.64 ± 3.30	197.11 ± 7.48	177.55 ± 2.21
9	349.50 ± 1.02	326.63 ± 8.54	267.19 ± 5.74	227.64 ± 3.30	197.11 ± 7.48	177.58 ± 2.33
10	416.77 ± 9.12	339.63 ± 5.20	280.07 ± 3.27	262.78 ± 5.21	234.64 ± 6.41	213.35 ± 7.15
10	416.77 ± 9.07	339.72 ± 5.39	280.07 ± 3.26	262.87 ± 5.32	234.64 ± 6.41	213.35 ± 7.14
10	420.34 ± 7.74	341.65 ± 4.93	288.84 ± 3.28	263.49 ± 2.40	236.20 ± 4.88	214.33 ± 4.85
10	420.47 ± 7.97	342.61 ± 4.39	288.85 ± 3.34	264.80 ± 4.38	236.20 ± 4.88	214.36 ± 4.72
10	421.81 ± 6.19	343.34 ± 4.17	296.62 ± 3.29	266.04 ± 3.50	237.47 ± 3.65	215.22 ± 3.98
10	422.37 ± 6.69	344.58 ± 3.60	296.67 ± 3.80	266.28 ± 2.67	237.47 ± 3.65	215.36 ± 3.39
10	423.60 ± 4.63	345.06 ± 2.13	303.38 ± 4.45	267.33 ± 2.12	238.40 ± 2.81	215.93 ± 7.42
10	424.32 ± 3.41	349.06 ± 2.41	303.51 ± 2.75	267.62 ± 3.71	238.42 ± 2.80	215.93 ± 7.43
10	424.72 ± 4.74	349.10 ± 3.53	309.03 ± 6.01	267.63 ± 1.70	238.96 ± 3.04	216.13 ± 4.76
10	425.64 ± 1.99	354.56 ± 2.50	310.74 ± 6.69	270.20 ± 2.90	239.07 ± 4.61	216.20 ± 4.84
10	425.86 ± 4.96	354.62 ± 2.33	310.94 ± 3.37	270.52 ± 2.24	239.12 ± 2.98	216.26 ± 3.03
10	426.50 ± 1.51	361.21 ± 2.73	313.87 ± 6.14	271.14 ± 1.47	239.20 ± 4.67	216.35 ± 2.41
10	426.59 ± 1.53	361.21 ± 2.74	315.20 ± 4.79	271.51 ± 1.61	239.58 ± 3.57	216.46 ± 3.92
10	426.72 ± 2.98	369.07 ± 3.87	318.46 ± 5.51	272.98 ± 1.44	239.65 ± 3.95	216.49 ± 4.05
10	427.00 ± 1.16	369.07 ± 3.87	318.56 ± 6.03	273.02 ± 1.44	240.07 ± 3.78	216.59 ± 3.01
10	427.05 ± 2.48	378.16 ± 5.69	320.47 ± 3.58	274.71 ± 1.89	240.21 ± 3.95	216.72 ± 3.26
10	427.07 ± 2.19	378.16 ± 5.69	321.04 ± 5.27	274.71 ± 1.89	240.34 ± 4.24	216.76 ± 2.22
10	427.15 ± 2.38	388.40 ± 7.93	324.70 ± 7.06	276.53 ± 2.82	240.51 ± 5.80	216.82 ± 2.33
10	427.42 ± 3.72	388.40 ± 7.93	325.21 ± 6.17	276.53 ± 2.82	240.54 ± 5.82	216.86 ± 2.89
10	427.71 ± 5.98	399.62 ± 10.38	325.58 ± 6.28	278.47 ± 4.10	240.84 ± 9.18	216.93 ± 2.81
10	427.71 ± 5.85	399.62 ± 10.38	325.90 ± 7.16	278.47 ± 4.10	240.85 ± 9.18	216.99 ± 2.80